35

Presented at CALOR97 Conference
Tucson, Arizona, Nov. 10-15,1997

BNL-65312
PX157

CONF-9711100--

The PHENIX PbSc Calorimeter and its Performance[a]

G.David, Y.Goto[b], E.Kistenev, S.Stoll, S.White, C.Woody
Brookhaven National Laboratory, Upton, New York

A.Bazilevsky, S.Belikov, S.Chernichenkov, A.Denisov, V.Kochetkov, Y.Melnikov, V.Onuchin, V.Semenov, V.Shelikhov, A.Soldatov, A.Usachev
Institute for High Energy Physics, Protvino, Russia

We have recently completed the production of the 15552 channel PbSc Electromagnetic calorimeter for the PHENIX experiment at RHIC. Our design features a single 4 tower module which is repeated throughout and which was produced with a number of QC steps designed to achieve consistent, large light yield in all channels. We present results on uniformity of the calorimeter, accuracy of a cosmic muon based precalibration scheme and test beam performance.

1 Introduction

The lead-scintillator electromagnetic calorimeter for the PHENIX experiment[1] is a shashlik type detector consisting of 15552 individual towers and covers an area of approximately 48 m^2. The calorimeter is used to measure electron and photon production in relativistic heavy ion collisions at RHIC, and will be an integral part of the particle identification and trigger system for PHENIX. In addition, the calorimeter will be used to measure high p_T photon production and other electromagnetic processes in high energy polarized proton collisions as part of the spin physics program at RHIC.

The calorimeter has a nominal energy resolution of $8\%/\sqrt{E(GeV)}$ and a timing resolution of $\leq$ 100 ps for electromagnetic showers [2]. An extensive precision calibration and monitoring system has been developed to achieve a predetermined absolute energy calibration of less than 5% for day one operation at RHIC, and to maintain an overall long term gain stability of better than 1%.

2 PbSc EMCal System Design

2.1 Optico-mechanical Design

The PbSc EMCal is built of optically independent readout towers containing 66 sampling cells, 1.5 *mm Pb* & 4 *mm Sc*, ganged together by penetrating

[a]This work was supported under DOE Contract DE-AC02-76CH00016
[b]Visitor from RIKEN (The Institute for Physical and Chemical Research), Wako, Saitama, Japan

DISCLAIMER

wavelength shifting fibers for light collection. Four towers are mechanically grouped together into a single structural entity called a module as shown in Fig. 1. Thirty six modules are attached to a backbone and held together by welded stainless steel skins on the outside to form a rigid supermodule.

A short summary of the major EMCal design parameters is given in Table 1

Table 1: Lead-Scintillator Calorimeter Parameters

Item	Parameters
Lateral segmentation	$5.535 \times 5.535\ cm^2$
Active cells	66
Scintillator	4 mm, Polystyrene (1.5% PT / 0.01% POPOP)
Absorber	Pb, 1.5 mm
Cell thickness	5.6 mm (0.277 X_o)
Active depth	375 mm
WLS fibers per tower	36
Fiber	BCF-99-29a, 1 mm
PMT type	FEU115M, 30 mm, MELS, Russia
Photocathode	Sb-K-Na-Cs
Luminous sensitivity	$\geq$ 80 μa/lm
Rise time (20%–80%)	$\leq$ 5 ns

2.2 Monitoring System Design

The calibration and monitoring system is based on a UV laser which supplies light to the calorimeter through a system of optical splitters and fibers. The block diagram of the monitoring system is shown schematically in Fig. 2[3].

Light from a high power YAG laser is initially split into six equal intensity beams using a set of partially reflecting mirrors. The beam from each mirror passes through a quartz lens and is focused to a point just in front of a quartz fiber which is used to transport the light over a distance of approximately 50 meters to each sector of the calorimeter.

A system of optical splitters is used to distribute the light to each of the individual calorimeter modules. The light is injected into a 38 cm long $\times$ 2 mm dia. plastic "leaky fiber" which allows the light to leak out of the fiber in such a way as to simulate a 1 GeV electromagnetic shower penetrating along the depth of the module. The overall efficiency to convert the primary light from the laser to photoelectrons in an individual module is of order 4×10^{-12}. Given

that the calorimeter has an intrinsic light output of $\sim$ 1500 photoelectrons per GeV, this leads to an energy requirement of $\sim$ 0.2 mJ per pulse from the YAG laser to deliver 1 GeV of equivalent energy to each tower.

2.3 Energy Calibration and Gain Monitoring

Construction of the calorimeter is now nearing completion. A precalibration scheme was developed which is based upon simultaneously recording the calorimeter response to cosmic μ's penetrating the supermodule in the direction nearly orthogonal to tower axis and the response due to laser exitation. A lego plot of the energies deposited by a penetrating μ inside the supermodule towers is shown in the bottom left corner of Fig. 3. The top left corner in the same figure is the energy spectrum in one tower exposed to laterally penetrating μ's. It peaks at 38 MeV and has a nearly gaussian shape with the $\sigma(E)/E$ ~30%. On average the EMCal towers produce 12500 γ's ($= \frac{1500\ ph.el.}{<QE>}$) per 1 GeV of deposited electromagnetic energy. The distribution of the light yield (normalized to an average value) for ~8000 towers is also shown in Fig. 3. Original light yield measurements are performed with a "standard set" of phototubes, whose QE's and gains differ from the actual tubes used in the final assembly. We use laser light amplitude to correct for QE and gain differences. When renormalization is made, the dispersion in the actual response of each tower to the original muon calibration is reduced to only 2.3%. This residual dispersion is due mainly to the nonuniformities in the quantum efficiencies of the phototubes over the active photocathode area, but is more than a factor of two better than the design goal of 5% in predetermining the initial energy calibration of the calorimeter for RHIC operation.

3 Test Beam Performance

3.1 Energy and position measurements

Pions up to $\sim$ 0.3 GeV/c and and protons up to $\sim$ 0.9 GeV/c are totally absorbed in the calorimeter. The line shapes measured in the calorimeter for 1 GeV/c π's, protons and electrons are shown in Fig. 4. Hadronic line shapes are nongaussian, with π's exhibiting a characteristic minimum ionizing peak at 270 MeV and a long tail extending towards the total available energy. Protons at 1 GeV/c nearly range out in the calorimeter and produce a straight through peak at $\sim$ 566 MeV. Both values are in agreement with the sampling fraction values as predicted from GEANT $\epsilon(e) : \epsilon(\pi) : \epsilon(p) = 0.19 : 0.27 : 0.31$. The 8% width of the energy distribution for electrons at 1 GeV agrees very well with our previously measured [2] energy resolution of:

$$\sigma(E)/E = 1.5 \oplus 8.0/\sqrt{E}, \qquad E(GeV),$$

and pion rejection factor ~ 100 for pion momenta above 2 GeV/c.
New measurements were made to improve the understanding of calorimeter response to particles spread over a wide angular range. Fig. 5 combines the simulated GEANT shower shape for three angles of incidence and GEANT predictions for the position resolution as function of the angle of incidence in the energy range $0.5 \div 8.0$ GeV/c and the experimental points measured in the test beam at the AGS. Both GEANT and the experimental data show that the shower projection onto the calorimeter front face becomes skewed at nonorthogonal angles of incidence. The data also show a gradual dilution of the shower core, mainly related to the longitudinal shower fluctuations contributing to the width of the projected shower. We found that the shower width depends on impact angle as

$$b(\theta) \ = b_0 + a(E) * sin^2(\theta),$$

where $b_0 = 7.8$ mm is an energy independent electromagnetic shower width for $\theta = 0$. The increased shower width for nonorthogonal angles of incidence results in improved position resolution for small angles (see insert). At a larger angles the contribution from longitudinal fluctuations becomes dominant and the position resolution degrades. All available data on position resolution can be well described by the simple formula

$$\sigma(X) \ = \sigma_0(E) + \Delta * sin(\theta),$$

where

$$\sigma_0(E) = 1.55 + \frac{5.7}{\sqrt{E}} \ (mm), \qquad E(GeV)$$

is the position resolution for normal incidence and $\Delta \ \sim \ L_{rad}$.

3.2 Effective mass measurements

A critical test of the calorimeter performance is its ability to measure multiphoton effective masses with good resolution. A typical 2γ effective mass distribution measured by exposing a single EMCal supermodule to neutral particles produced from interactions of 7 GeV/c π^-'s in a plexiglass target upstream of the calorimeter is shown in Fig. 6. A summary of the π^0 mass measurements together with results of the GEANT simulation is given in Table 2.

Table 2: π^0 mass measurements in EMCal

Beam Momentum (GeV/c)	3	5	5	7
Distance from Target (cm)	169	169	239	239
Test Beam Data				
Fitted π^0 mass (MeV)	133.1	134.1	137.1	135.6
	±0.8	±0.5	±1.0	±0.4
σ of the fit (MeV)	15.0	16.3	12.1	14.6
	±0.7	±0.5	±0.9	±0.4
GEANT predictions				
Fitted π^0 mass (MeV)	134.9	135.3	135.2	134.8
σ of the fit (MeV)	13.2	15.8	11.5	13.8
σ(X) Contribution (MeV)	9.0	13.5	8.6	12.1
σ(E) Contribution (MeV)	8.0	7.2	6.5	6.4

3.3 Time of Flight Measurements with Calorimeter

The interest in the timing resolution of the calorimeter is stimulated by the idea of using timing information as a particle identification tool and for pattern recognition. The differences in the light and shower propagation speeds in the calorimeter result in the PMT seeing the light from the last tile nearly 1.5 ns earlier than from the first tile. Combined with the type and energy-dependent showering characteristics it results in systematic differences between arrival times of electrons and hadrons. Fig. 7 summarizes the data on systematic differences between arrival times for μ's, π's and p's at three momenta. Towers with low deposited energies (periphery of the showers) see hadrons delayed with respect to electrons. However penetrating particles and fully developed hadronic showers produce a timing signal $\sim 200ps$ earlier than electrons.

The timing resolution curves (stochastic term) plotted in Fig. 8 combine the points measured exposing the calorimeter to the particles in the 0.3 - 1 GeV/c momentum range. The timing resolution for very low deposited energies is driven by the proximity of the maximum signal amplitude to the threshold on the timing discriminator. Away from the discriminator threshold the calorimeter timing resolution is nearly constant ($\sim 100ps$ for electrons, $\sim 200ps$ for hadrons) due to the fact that shower fluctuations are the major contributor to the measured *rms* values. In general, the data can be well fitted by the function:

$$\Delta t = \Delta t_0 + \Delta t_1/(E - E_{threshold}), \qquad E\ GeV/c,$$

which includes a pole type divergence close to the threshold. Here Δt_0 is an intrinsic timing resolution limit, presumably due to fluctuations in the localization of the shower, and Δt_1 includes contributions due to photon statistics and pulse shape fluctuations. The latter is dominant close to threshold, and may be tuned by adjusting the gain of the phototubes and discriminator thresholds.

4 Summary

We have designed and successfully constructed a 15 552 channel electromagnetic calorimeter covering total area of 48 m^2 using an approach which was optimized for industrial mass production. We relied heavily on industrial style quality control procedures to insure conformity to physics specifications.
The calorimeter has a light yield of $\sim 12500\gamma/GeV$ of electromagnetic energy. The calorimeter has energy and position resolutions ~8% and ~7 mm respectively for 1 GeV photons and electrons at normal incidence and gives a π^0 mass with resolution of ~15 MeV.
It has an excellent timing resolution of ~100 ps for electromagnetic and ~200 ps for hadronic showers which is nearly independent of the energy well above threshold. We believe that in addition to providing PHENIX with measurements of photon and electron probes of the QGP, the excellent timing performance of EMCal will greatly enhance the capabilities of PHENIX for studying the QGP via hadronic probes.

1. PHENIX Conceptual Design Report, BNL 48922, January 29, 1993
2. E.Kistenev et.al.,"PHENIX PbSc Electromagnetic Calorimeter: Results of Test Beam Studies", *Proceedings of the Fifth International Conference on Calorimetry in High Energy Physics* World Scientific (1994) 211-223.
3. G.David et.al.,"The Calibration and Monitoring System for the PHENIX Lead-Scintillator Electromagnetic Calorimeter", *IEEE Trans. Nucl. Sci.* (1997) submitted for publication.

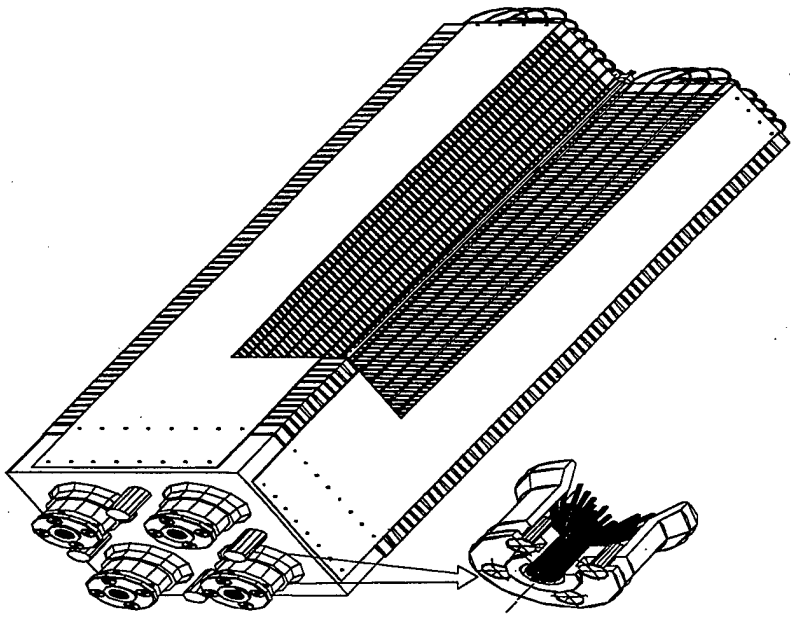

Fig. 1: Interior view of a calorimeter module showing the stack of scintillator and lead plates, wavelength shifting fiber readout, and leaky fiber inserted in the central hole

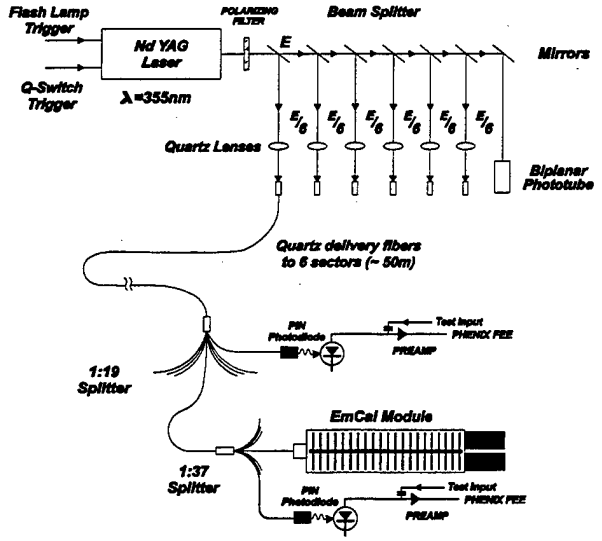

Fig 2: Laser calibration, monitoring and light distribution system

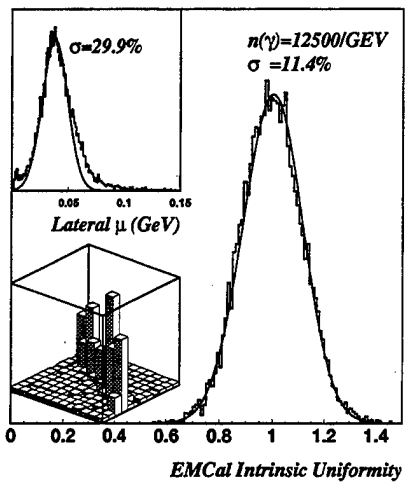

Fig 3: Uniformity of the Light Yield in the PHENIX EMCal. Inserts: (top) - Energy distribution in EMCal towers exposed to laterally penetrating cosmic μ's; (bottom) - Lego plot of energies deposited in EMCal towers by laterally penetrating cosmic μ's.

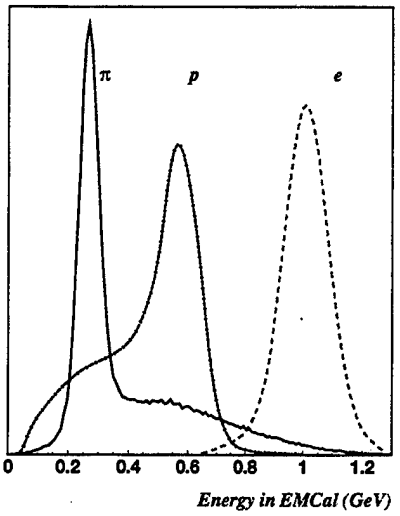

Fig. 4: EMCal response to 1 GeV/c π's, protons and electrons

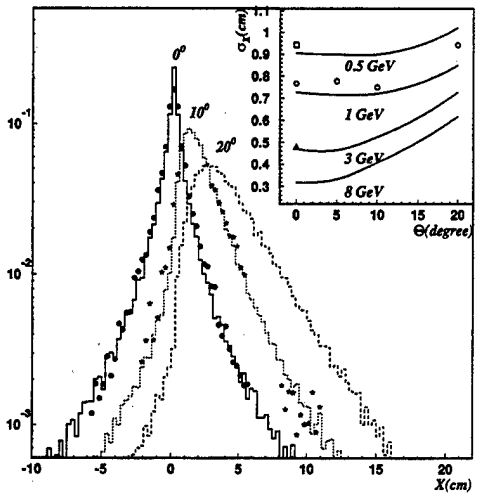

Fig. 5 : Projected shower shapes for 1 GeV electrons for different angles of incidence (histogram and curves - GEANT, points - test beam). Insert: EMCal position resolution.

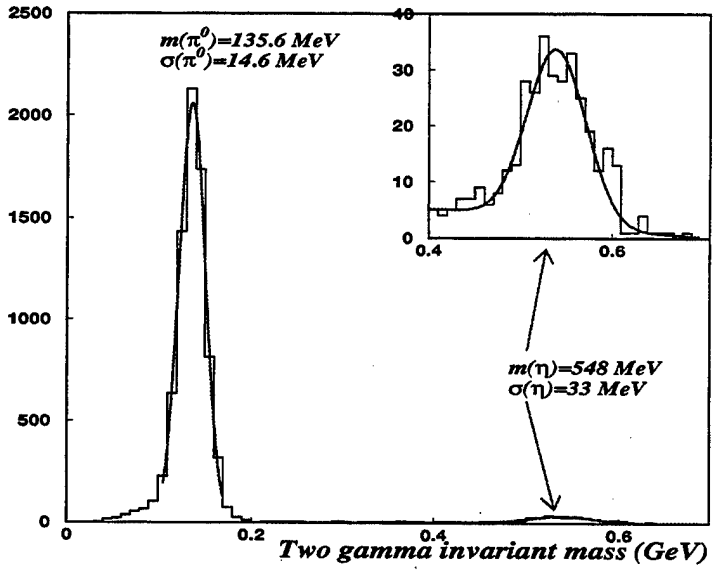

Fig. 6: Two-photon effective mass distribution measured by exposing a single EMCal supermodule to a beam of negative π's with a target ~ 3 m upstream of the calorimeter.

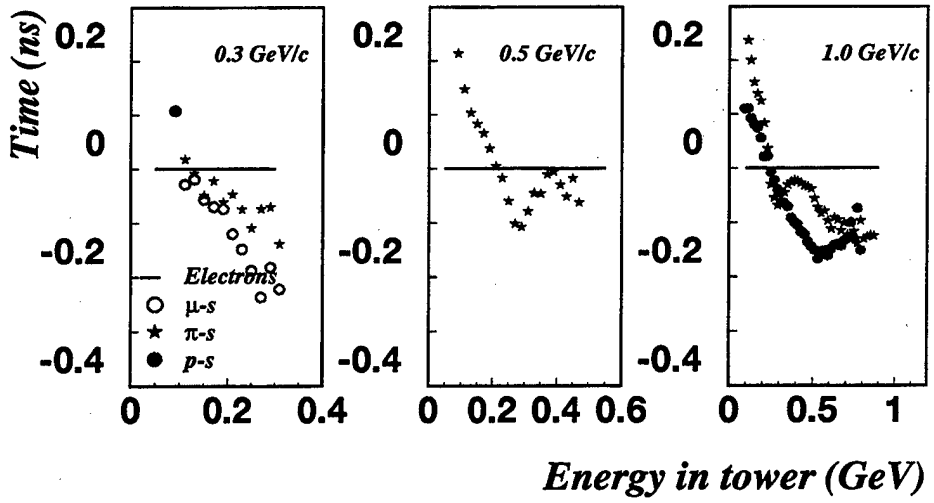

Fig. 7: Arrival times measured by the EMCal for different particles (with respect to electrons of a similar momenta) as a function of the energy deposited in the tower used for timing measurements.

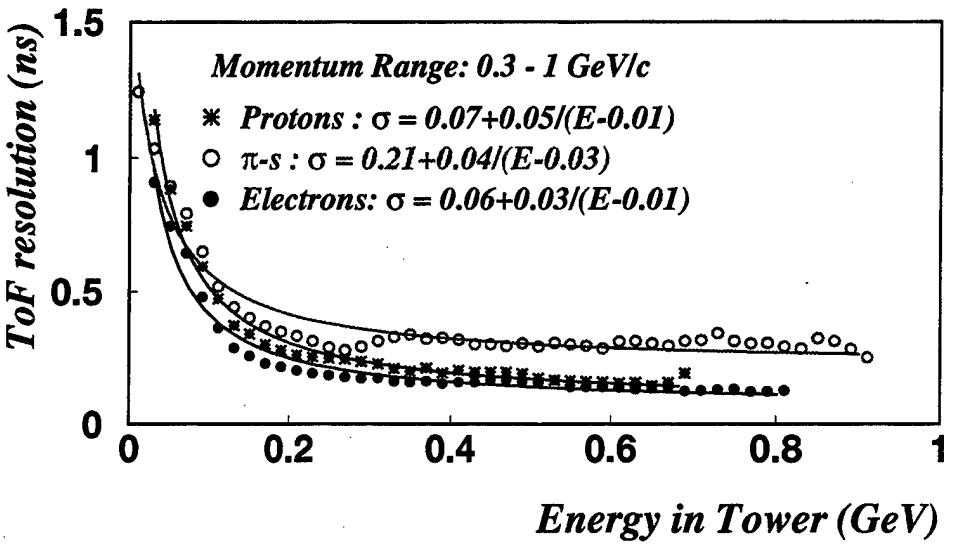

Fig. 8: EMCal timing resolution for different particles in the momentum range 0.3÷1 GeV/c

Report Number (14) BNL--65312
CONF-9711100--

Publ. Date (11) 199711
Sponsor Code (18) DOE/ER, XF
UC Category (19) UC-414, DOE/ER

DOE